UNIVERSIDAD
NACIONAL
DE COLOMBIA

Coffee plantation soil characterization using a multi-method approach near the Volcano Nevado del Ruiz, Colombian Central Cordillera

Brayam Hincapié[1], Alexander Cortés-Soto[1], Mauricio A. Bermúdez[2]*, Santiago Yepez[3], Juan Sebastián Trujillo-Hernández[1], Blanca Myriam Salguero-Londoño[1], Sebastián Grande[4],

[1]Universidad de Ibagué, Colombia

[2]Universidad Pedagógica y Tecnológica de Colombia (UPTC)

[3]Universidad de Concepción, Departamento Manejo de Bosques y Medio Ambiente, Chile

[4]Departamento de Geología, Universidad Central de Venezuela

*Corresponding author: mauricio.bermudez@uptc.edu.co

ABSTRACT

The presence of iron oxides may provide a sensitive indicator of the effects of cropping practices on coffee plantations. Authors characterized the mineral phases present in soil A horizons at three different farms located in the Department of Tolima within the regions of Líbano and Villahermosa. Our analysis includes X-ray diffraction, Mössbauer spectroscopy, and remote sensing to discriminate the distribution of the different magnetic mineral phases. X-ray diffraction was used to identify the mineralogical properties of iron oxide such as hematite, goethite, and ferrihydrite (Fh), as well as tectosilicate minerals such as albite and sanidine. Mössbauer spectroscopy results for samples taken at room temperature indicate the presence of Fe^{2+} and Fe^{3+} mineral phases, which possibly correspond to ilmenite or magnetite. Finally, Sentinel-2A multi-spectral imager (MSI) data was used to map the distribution of iron oxides and study the influence of their distribution throughout the study area. A high correlation between Mössbauer spectroscopy and Sentinel-2A MSI data exists throughout the study area. The results suggest that farms close to the main Nevado del Ruíz Volcano have a more significant mineralogical variability. In contrast, more distant farms are characterized by soils with more iron oxides, the product of weathering, erosion, and human activities.

Caracterización de suelos cercanos al Volcán Nevado del Ruíz, Cordillera Central de Colombia, con técnicas multiherramientas

RESUMEN

La identificación de óxidos de hierro puede proporcionar un indicador sensible para determinar los efectos de diferentes prácticas de cultivo en plantaciones de café. Por tal razón, en la presente investigación se analiza el suelo de tres fincas ubicadas en el Departamento del Tolima. Se caracterizaron las fases minerales con hierro a lo largo de la capa productiva (horizonte A) de los suelos en las regiones de El Líbano y Villahermosa. Se utilizó difracción de rayos X, espectroscopia de Mössbauer y teledetección para discriminar la distribución de las diferentes fases minerales magnéticas. La difracción de rayos X se utilizó para identificar las propiedades mineralógicas del óxido de hierro como la hematita, la goethita y la ferrihidrita (Fh), además de los minerales tectosilicatos como la albita y la sanidina. Los resultados de la espectroscopia de Mössbauer para muestras tomadas a temperatura ambiente indicaron la presencia de fases minerales de Fe^{2+} y Fe^{3+}, que posiblemente corresponden a ilmenita o magnetita. Finalmente, se utilizaron datos y anchos de banda de Sentinel-2A MSI para mapear los óxidos de hierro y estudiar la influencia de su distribución en toda el área de estudio. Los datos encontrados a través de las distintas técnicas, difracción de rayos X, espectroscopia de Mössbauer, y la comparación con datos Sentinel-2ª, son muy consistentes a lo largo del área de estudio. Nuestros resultados sugieren que las fincas cercanas al principal volcán Nevado del Ruíz tienen una mayor variabilidad mineralógica. En contraste, aquellas que se encuentran más distantes presentan una mayor cantidad de óxidos de hierro, producto de la erosión y las actividades humanas.

1. Introduction

Colombia's Coffee Axis, called in Spanish "Eje Cafetero" is a famous coffee region located near the intersection of four administrative regions (departments): Caldas, Quindío, Risaralda, and Tolima, along the foothills of the Los Nevados National Park. The Coffee Axis is renowned for growing and producing most Colombian coffee, considered to be the best in the world. Most of the population in the Eje Cafetero depends on coffee production. Farmers in the region apply different cropping practices (organic practices and traditional cultivation). This variety in cultivation techniques is thought to bring a unique characteristic to Colombian coffee. Different factors influence crop growth and yield (Reddy et al., 2003; Kang et al., 2009; Zhang et al., 2001). Internal factors associated with plants (genetic) and environmental or external factors (climatic, edaphic, biotic, physiographic, socio-economic, chemical, and physical) affect crop growth and yield. Inadequate nutrients result in low crop production, increased disease, and decreased plant resistance to pests. In these cases, soil intervention and the use of agrochemicals are necessary. Iron plays an essential role in respiration, photosynthesis, and the production of healthy green leaves (Rout & Sahoo, 2015). Iron can be considered a micro-nutrient because only small amounts are required. Iron deficiency produces chlorosis and stunted growth. In contrast, although not common, iron in excessive quantities could produce toxicity, with symptoms including bronzing, discoloration, and stippling of leaves. Soil pH influences the availability of micronutrients (Boron, Iron, Zinc, Copper, and Manganese) (Khadka, 2016). Iron toxicity is a frequent problem in acid soils (Nenova, 2006).

Soil pH has a dominant effect on solubility and, therefore, availability and potential phytotoxicity of ions (nutrients and toxic elements) (Clark and Baligar, 2000). Some plants secrete acids from their roots that decrease soil pH-value and inducing iron deficiency, reported as a common problem (Shenker and Chen, 2005). While most of the iron in soils is ferric (Fe^{3+}), ferrous iron (Fe^{2+}) is more important from a physiological point of view (Hernández and Muerer, 1997).

Due to its low solubility, the plant roots have access to Fe^{2+} or Fe^{3+} ions; thus, some mechanisms are employed to reduce the Fe^{3+} ion to Fe^{2+} ion before reaching the root crossing the selective membranes (Colombo et al., 2013). Fe^{3+} is insoluble in soils with neutral or high pH, which means it is not available for plants in alkaline and calcareous soils. In addition, iron in this type of soil is easily incorporated in phosphates, carbonates, and hydroxide ions (Lindsay, 1991).

Changes in soil chemical properties are the result of different input cropping practices (Clark et al., 1998). The identification of iron oxides may provide a sensitive indicator of the effects of cropping practices on coffee plantations. Distribution and abundance of oxides and minerals may affect the nature of the coffee crop. Magnetic characterization of coffee crops soils can be studied using Mössbauer spectroscopy technique to identify different compounds, hydroxides, and iron oxides. Additionally, X-ray diffraction is applied identify the mineralogy of both parent material and authigenic minerals in the soil.

In cropping practices management, soil oxides identification can be useful to develop effective strategies for sustainable management, especially in a scenario of increasing shortage of mineral phosphate resources (Fink et al., 2016). This study allows the characterization of the soils of the farms studied using multi-tool techniques. When this information it is integrated with production rates it is possible to infer the relationship among the different cropping practices techniques used for coffee cultivation, soil type and crop management.

High iron levels often cause manganese deficiency in a plant because of the competitive ionic behavior of the two micronutrients. Manganese deficiency exhibits similar symptoms as iron deficiency, such as yellowing of leaves, except that manganese deficiency affects both young and old foliage, while iron deficiency affects only young foliage. Iron and manganese toxicity have similar symptoms in plants as well (Li & Lan, 2017).

Iron anomalies, such as: iron ore deposits, can be detected using remote sensing techniques such as Landsat ETM+ (Ciampalini et al., 2013). As the strong pigmenting effect of Fe oxides gives most soils their color, a first mapping of iron oxides was carried out in 1984 using coarse resolution Landsat multispectral scanner (MSS) data. Subsequently, with the advent of 30 m Landsat Thematic Mapper (TM), different bandwidths were established to separate argillic and non- argillic materials (using near infrared 5/7 bands) with the objective to map ferric /ferrous oxides (using visible 3/1 TM bands) (van der Werff and van der Meer, 2016).

Since 2000, the 14-band, 20 m pixel resolution ASTER sensor on the TERRA satellite has been used extensively in geological application studies for surface mineralogy mapping. To provide continuity with order Landsat data, a subset of ASTER bands overlap with those of Landsat TM, as do the Sentinel-2A MSI bands. The Sentinel-2 is an Earth observation mission from the European Union Copernicus Program, which acquires in a systematically way optical imagery at high spatial resolution often between 10 m to 60 m over land and coastal waters.

In this research, we discriminate between iron oxides and overall mineralogy at different scales. At the scale of a soil pit, we use Mösbauer spectroscopy and X-ray diffraction to detect different mineral species in soils from three farms, with different cropping practices, this allow us to evaluate the impact of such methodologies on soil oxidation processes. Remote sensing analysis using Sentinel-2A MSI data, combined with detailed soil pit mineralogy from the farms, allows us to scale up observations across the landscape. In addition, results of this study provide information to determine the influence of other geological processes such as lahars, and others erosion processes.

2. Study area

Authors chose two coffee-growing municipalities located in northern Tolima Department, Colombia: 1) the Líbano municipality, and 2) the Villahermosa municipality (Figure 1). Average elevation of the study area is 2079 meters above sea level (m.a.s.l) with variables slopes (medium to high) where coffee is cultivated. In these municipalities, soils are poorly developed,
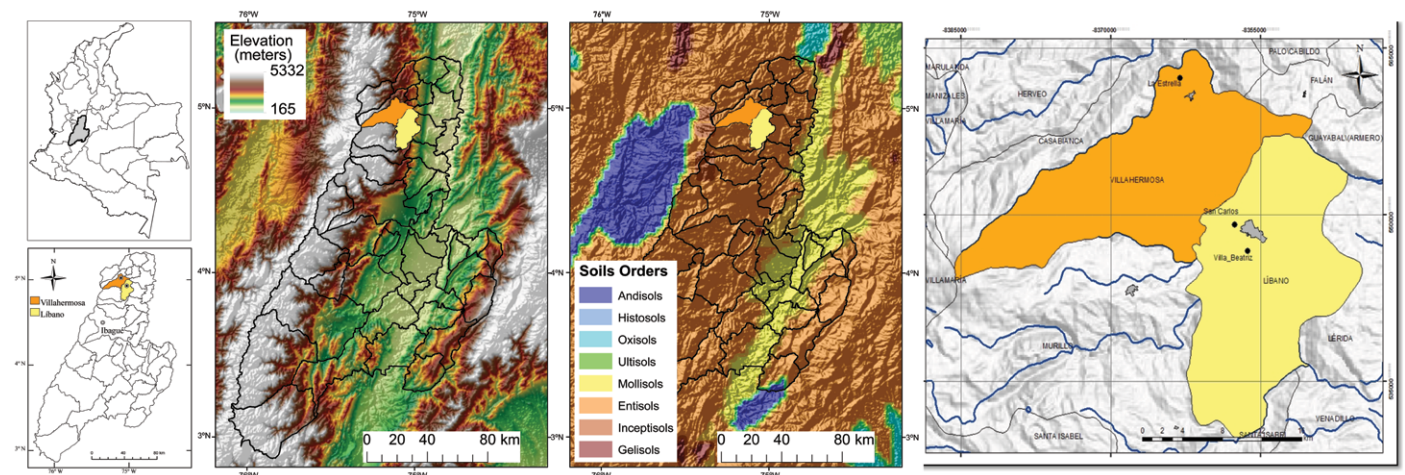
Figure 1. Location of the study area and maps of soils. Map of soils is based on the NRCS Soils database (Eswaran and Reich, 2005).

Coffee plantation soil characterization using a multi-method approach near the Volcano Nevado del Ruiz, Colombian Central Cordillera

265

characterized by weak horizon development, and are classified as inceptisols (Eswaran and Reich, 2005; Figure 1).

2.1 Sampling and pretreatment of samples

Samples were collected from three different sites and production systems: Villahermosa (orange polygon, Figure 1) and San Carlos farm in the municipality of Líbano (yellow polygon, Figure 1), where different cropping practices (conventional and best agricultural practices; BAP) are applied. Figures 2 provides visual context for the three farms selected for this study.
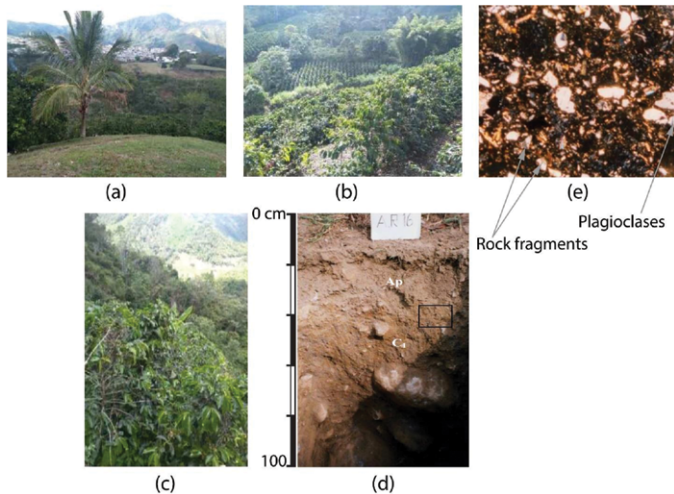
Figure 2. Sampling sites: (a) Villa Beatriz, (b) San Carlos, and (c) La Estrella farms. (d) Example of the soil located to the north of the farm La Estrella. (e) Thin section of the soil, photo taken to 4X and polarized light (d and e graphics were modified with permission from Guarin, 2004).

According to procedures established by the Colombian Agricultural Institute (ICA; CCDIA, 2005), thirty (30) samples were taken from the productive soil layer (A-horizon) during the summer season between October and November, 2015 from a patch of approximately 562,500 m^2 (five hundred coffee plants in each line; Figure 3a), these were selected and marked with a color ribbon for repeated visits. We applied the same methodology in each farm (Figure 3), for a total of ninety (90) samples. We discriminated the A-horizon

(between 30 to 35 cm depth) by a thin dark layer formed by organic matter, altered or partially altered, where remains of animals, leaves, and branches among others can also be observed (CCDIA, 2005). This layer is characterized by an abundance of minerals because of the erosion of the surrounding mountains.

3. Materials and methods

The following materials were used for the sampling procedure: a clean bucket, a drill bit, a shovel, cardboard boxes, and plastic bags. We scraped off the upper centimeter of the soil surface to remove fresh residues of organic matter, road dust or other artificial contamination. A V-shaped hole was dug approximately as wide as the width of the space, a depth of 30-35 centimeters was considered, depending on the location. A 2 to 3-cm thick slice of soil was cut into the wall of the trench and a 3 to 5-centimeter-wide strip was taken from the center of that slice. This strip of soil was placed in the bucket and the operation was repeated in each location. The extracted soil samples were mixed to roughly homogenize the individual samples with a subset retained and approximately 500 g discarded back into the pits. Preserved at room temperature, the samples were hygienically separated and stored in flasks to be sent to the corresponding laboratories for analyses.

3.1 Chemical Parameters

Chemical parameters in the same farms studied here, were measured successively using the same exact methods and in the same laboratories during two dry and rainy seasons. Among the measured parameters are pH, Cation Exchange Capacity (CEC), Soil Organic Matter (SOM), phosphorus expressed as phosphorus pentoxide (P_2O_5) and potassium expressed as potassium oxide (K_2O).

3.2 X-Ray Diffraction

This technique was used to identify the mineral phases present in the soil samples. X-ray diffraction measurements were made in the CETENE (Strategic Technologies Center Northeast) in the state of Pernambuco, Brazil. We did the X-ray diffraction (XRD) analysis for the soil using a Shimadzu XRD-6000 X-ray diffractometer with Cu radiation - Kα (λ = 1.54056 Å), and a 40kV. Tests were carried out at a temperature of 298K and 30 mA current and the measurements were acquired at angular intervals $0^o \leq 2\theta \leq 120^o$, compass $\Delta(2\theta)$ = 0.02°Δt/ and step (2θ) = 4s representing a total acquisition time of 14 h 34 min 17s.
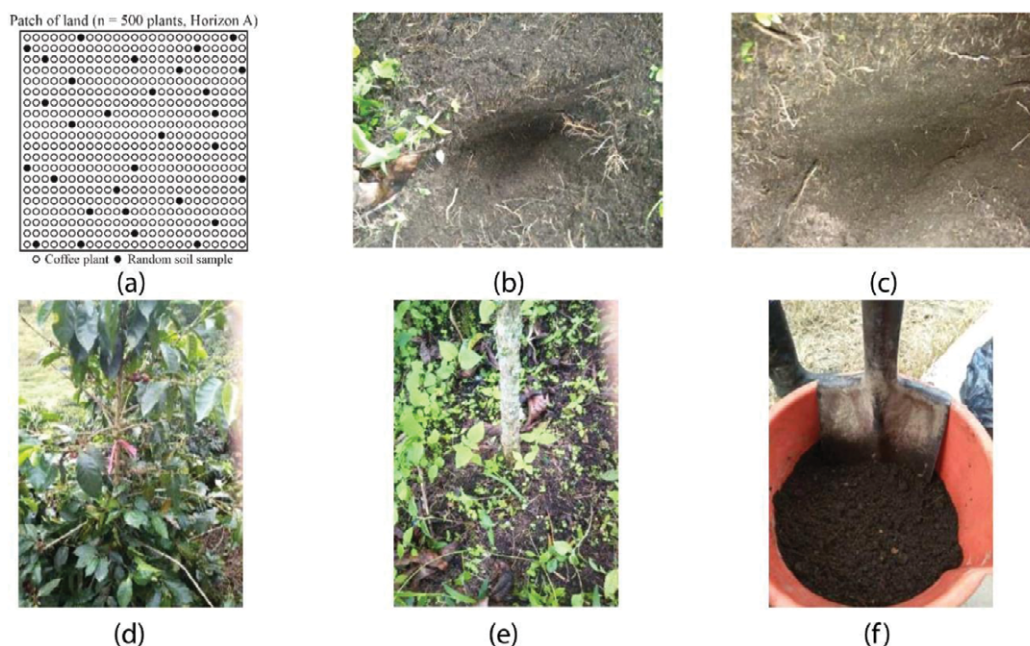
Figure 3. (a) Sampling strategy, (b) Villa Beatriz farm's soil. (c) San Carlos farm's soil. (d) Coffee plant with red ribbon. (e) Stem of the coffee plant, and (f) collected soil sample.

3.3 Mössbauer Spectrometry

The samples were measured in a transmission Mössbauer spectrometer using a Co-57/Rh source in the Mössbauer Spectroscopy Laboratory, of the Physical Metallurgy and Phase Transitions Theory Group of the Universidad del Valle, Colombia. Between 512 and 1024 channels were used for spectrum storage. The spectra were fitted by using the MOSFIT program (Varret and Teillet, 1976; Larson and Von Dreele, 2004); and pure α-Fe was used for calibration. Mössbauer spectroscopy has advantages over X-Ray diffraction in everything related to the identification of minerals containing Fe as a selective technique (Byrne and Kappler, 2019).

3.4 Sentinel-2A data processing

In this study a Sentinel-2A MSI L1C image was used, which was downloaded from the European Space Agency (ESA) through the Sentinel Scientific Data Hub (https://scihub.esa.int/dhus/). The spatial resolution of Sentinel-2A MSI is dependent on a spectral band. There are 13 spectral bands, from the visible and the near infrared to the shortwave infrared, at different spatial resolutions ranging from 10 to 60 meters on the ground. The four bands at 10-meter resolution are normally used for basic land-cover classification. The other six bands, at 20-meter resolution, are used to obtain geophysical parameters, whereas the bands at 60-meter resolution are mainly dedicated to atmospheric corrections and cirrus-cloud screening. Before using the Sentinel-2A MSI LC1 dataset we performed a series of pre-processing tasks: 1) An atmospheric correction was implemented using Sen2Cor (software version 2.5.5), and 2) A combination of bands, resampled to 20 m resolution.

Different bandwidth of electromagnetic radiation, or ratios of bands serve as indicators for mineral sets or mineral groups. Table 1 provides an overview of the Landsat 5 TM and ASTER bandwidth suitable for use with Sentinel-2A MSI. We focus on bands originally defined for Landsat 5 TM by Sabins (1999), which require Sentinel-2A MSI bands 2, 4, 11 and 12. Additionally, the band 8a of the Sentinel-2A MSI was required for masking vegetation using the NDVI result.

Three bandwidths, defined in Table 1, were selected for mapping the alteration of the mineralogy around the regions defined as study areas in the Tolima department in Colombia. This combination highlights hydroxyl bearing alteration (S-2A MSI 11/12), discriminates iron oxides in general (S-2A MSI 4/2), and emphasizes ferrous iron oxides specifically (S-2A MSI 4/11). Finally, the mineral alteration map obtained from Sentinel-2A MSI was compared with the spatial locations of each of the three farms where the samples were collected.

Table 1. Bandwidth applied in Sentinel-2A MSI as proxies for mapping mineralogy (Modified after van der Werff and van der Meer, 2016)

Parameter to discriminate	Bandwidth
Landsat 5 TM ratios (Compatible with Sentinel 2A-MSI)	
Hydroxyl bearing alteration	11/12
All iron oxides	4/2
Ferrous iron oxides	4/11
ASTER Iron	
Ferric Iron, Fe^{3+}	4/3
Ferrous Iron, Fe^{2+}	12/8 + ¾
Laterite	11/12
Gossan	11/4
Ferrous silicates	12/11
Ferric oxides	11/8
ASTER Silicates	
Alteration	11/12
ASTER Other	
Vegetation	8/4
NDVI	(8 - 4)/(8 + 4)

4. Results

4.1 Chemical Parameters

Table 2 summarize the results found during the dry and rainy seasons, respectively. The measurements for the rainy season were carried out from May to August 2015, whereas for the dry season they were accomplished between August and December 2015. This table present the mean values, and the standard deviation (SD).

During the rainy season, La Estrella farm, with organic practices system, recorded the highest mean pH value (5.3); San Carlos farm, with BAP system, presented a pH mean value of 5.2 ± 0.3; and Villa Beatriz farm, with conventional system practices, obtained mean pH values of 5.1 ± 0.2, being all these values within the normal pH range for coffee cultivation (5 - 5.5; Sadeghian, 2008).

Concerning the CEC, Villa Beatriz farm gave a value of 19.7 ± 0.6 meq/100 g, San Carlos and La Estrella farms presented values of 18.0 ± 3.0 and 17.7 ± 3.1 meq/100 g, respectively.

For the SOM parameter, Villa Beatriz farm obtained a mean value of 2.3 ± 0.1%, followed by La Estrella farm with 2.1 ± 0.3% and San Carlos with 2.0 ± 0.2%. All these values are less than 5%, which are considered low for coffee production (Sadeghian, 2008).

Regarding the phosphorus oxide (P_2O_5) content, La Estrella farm gives mean values of 52.7 ± 5.5 ppm, San Carlos farm registers the highest mean value with 25.3 ± 12.7 ppm followed by Villa Beatriz with 21.7 ± 10.2 ppm. These values are all within the optimal range considered for coffee production (Sadeghian, 2008).

Table 2. Chemical parameters evaluated in three (3) farms with different coffee production systems during the rainy season (May-August 2015) and the dry season (August-December 2015).

Farm and/or productive system	Parameter	Mean[r]	SD[r]	Mean[d]	SD[d]
San Carlos (BAP)[1]	pH	5.2	0.3	*5.1*	*0.3*
	CEC (meq/100 g)	18.0	3.0	*15.7*	*0.6*
	SOM (%)	2.0	0.2	*1.7*	*0.1*
	P_2O_5 (ppm)	25.3	12.7	*29.0*	*11.5*
	K_2O (ppm)	22.7	7.4	*11.3*	*3.1*
Villa Beatriz (CS)[2]	pH	5.1	0.2	*5.1*	*0.1*
	CEC (meq/100 g)	19.7	0.6	*19.3*	*0.6*
	SOM (%)	2.3	0.1	*2.0*	*0.1*
	P_2O_5 (ppm)	21.7	10.2	*34.7*	*3.8*
	K_2O (ppm)	12.1	0.8	*25.8*	*10.6*
La Estrella (OP)[3]	pH	5.3	0.0	*5.0*	*0.1*
	CEC (meq/100 g)	17.7	3.1	*20.7*	*4.0*
	SOM (%)	2.1	0.4	*2.0*	*0.1*
	P_2O_5 (ppm)	52.7	5.5	*43.0*	*3.0*
	K_2O (ppm)	18.0	7.4	*9.4*	*3.5*

BAP[1]: Best Alternative Practices, CS[2]: Conventional System, OP[3]: Organic Practices. Superscripts r and d correspond to rainy and dry season, respectively.

Concerning the potassium oxide (K_2O), Villa Beatriz farm provides the lowest mean value with 12.1 ± 0.8 ppm, San Carlos with 22.7 ± 7.4 ppm and La Estrella 18.0 ± 7.4 ppm. However, all these values are within the normal range of K_2O (7.8 – 27.4 ppm) according to Sadeghian (2008).

The pH parameter during the dry season for La Estrella farm has a mean value of 5.0 ± 0.1, San Carlos farm with 5.1 ± 0.3 and Villa Beatriz farm with 5.1 ± 0.1. For the CEC, La Estrella has the highest mean value with 20.7 ± 4.0 meq/100g, followed by Villa Beatriz farm with 19.7 ± 0.6 meq/100gr and San Carlos farm with 15.7 ± 0.6 meq/100g. Concerning the SOM parameter, the results obtained were: San Carlos 1.7 ± 0.1%; Villa Beatriz 2.0 ± 0.1%; and La Estrella 2.0 ± 0.1%, respectively. For the P_2O_5, San Carlos farm exhibits the lowest mean value with 29.0 ± 11.5 ppm. Villa Beatriz farm with 34.7 ± 3.8 ppm, and La Estrella farm with 43.0 ± 3.0 ppm. For the K_2O, Villa Beatriz exhibits the highest mean values of 25.8 ± 10.6 ppm; San Carlos with 11.3 ± 3.1 ppm, and La Estrella with 9.4 ± 3.5 ppm.

Coffee plantation soil characterization using a multi-method approach near the Volcano Nevado del Ruiz, Colombian Central Cordillera

267

4.2 X-Ray Diffraction

Figure 4 shows X-ray diffractograms for the three samples: D1 (Villa Beatriz), D2 (San Carlos), and D3 (La Estrella), which were discriminated using the American Mineralogist Crystal Structure Database (Downs and Hall-Wallace, 2003). Peaks of different intensities are associated with the presence of various minerals containing iron oxides in its structure, such as: hematite, goethite and ferrihydrite. Other minerals without iron in their chemical composition were also identified, such as: illite, quartz, Na-feldspar, K-feldspar, calcite, albite-oligoclase (Table 3).

Table 3. Common minerals identified by X-rays diffraction.

Abbreviation	Mineral	Chemical Formula	Category
Q	Quartz	SiO_2	Mineral oxide
G	Goethite	$\alpha\text{-}FeO^{3+}(OH)$	Mineral oxide
FNa	Na-feldspar	$(Na,Ca)(Si,Al)_3O_8$	Mineral tectosillicate
H	Hematite	Fe_2O_3	Mineral oxide
M	Muscovite	$KAl_2(AlSi_3O_{10})(OH)2$	Mineral phylosillicate
I	Illite	$(K,H_3O)(Al, Mg, Fe)2(Si, Al)_4O_{10}[(OH)_2,(H_2O)]$	Mineral phylosillicate
S	Sanidine	$K(AlSi_3O_8)$	Mineral tectosillicate
C	Calcite	$CaCO_3$	Mineral
F	Ferrihydrite	$Fe_{10}{}^{3+}O_{14}(OH)_2$	Mineral oxide

Table 4. Crystallographic information of the peaks of mineral phases found in sample D1

Mineral name	Position	Intensity	Miller Index (H K L)	I.D (A)
Ferrihydrite (F)	18.0545	0.183	0 0 2	4.91
Quartz (Q)	20.8173	0.2812	1 0 0	4.26
Goethite (G)	21.8953	0.4667	1 0 1	4.05
Na-feldspar (FNa)	22.8278	0.5744	1 0 0	3.84
Calcite (C)	23.6601	0.6568	0 1 2	3.76
Hematite (H)	24.4236	0.9736	0 1 2	3.68
Quartz (Q)	26.6669	0.4633	1 0 1	3.34
Illite (I)	26.6693	0.3261	0 2 2	3.34
Muscovite (M)	27.7562	0.4949	1 1 4	3.2
Calcite (C)	29.5205	0.4351	1 0 4	3.02
Illite (I)	30.2548	0.3595	-1 1 3	2.95
Calcite (I)	31.4365	0.3946	0 0 6	2.84
Muscovite (M)	32.8954	0.2844	-1 1 6	2.79
Illite (I)	35.608	0.2927	0 0 4	2.52
Ferrihydrite (F)	36.7349	0.1536	1 0 1	2.44
Quartz (Q)	39.267	0.2425	1 0 2	2.29
Quartz (Q)	42.5529	0.6747	2 0 0	2.12
Illite (I)	44.9159	0.2626	-2 2 3	2.01
Goethite (G)	51.4516	0.3527	4 1 1	1.67
Quartz (Q)	54.7409	0.1802	0 2 2	1.65
Goethite (G)	57.0544	0.1686	3 1 2	1.61
Calcite (C)	60.0971	0.1618	2 1 4	1.53
Ferrihydrite (F)	61.3733	0.1748	1 0 5	1.51
Illite (I)	62.5602	0.1748	3 3 0	1.44
Quartz (Q)	68.2671	0.1748	0 3 1	1.37

There are peaks of minerals associated with sample D1: the presence of iron oxides such as hematite, goethite and ferrihydrite, of which a peak of maximum intensity (0.9736) is observed on the diffractogram (Figure 4a; Table 4), this denotes the presence of hematite with an interplanar distance of 3.68 Å. Goethite has reflections along the diffractogram with variable intensities, ferrihydrite is present in very low amounts based on the diffractogram peaks intensities of the samples quartz and illite peaks, with intensities of 0.4633 and 0.3261, respectively, are observed with an interplanar distance of 3.34 Å. Quartz is abundant in all the samples, with several peaks visible in the diffractogram. The detection limit of the Shimadzu XRD-6000 permits determining if the peak is present, thus no reflection in Bragg diffraction (intensity of diffracted radiation) permits to discrimination of quartz, muscovite, calcite and illite. As in the case of hematite, Na-feldspar was also detectable.
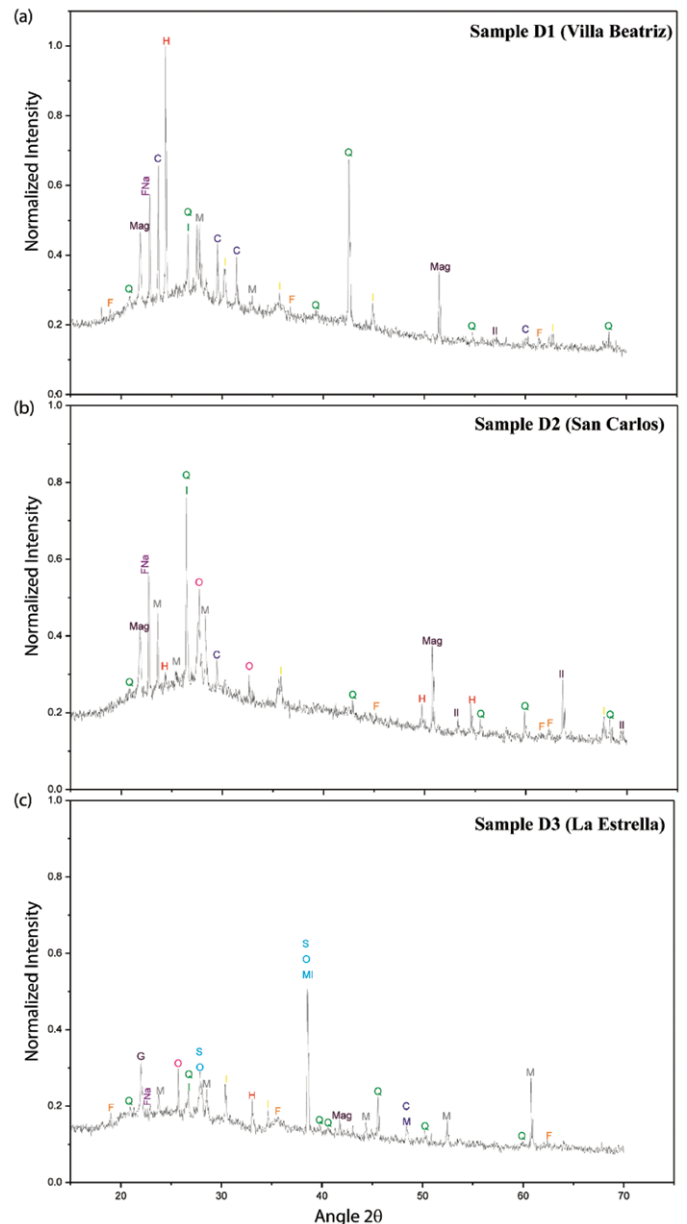
Figure 4. X-ray diffractograms of soil A horizon samples of coffee crops soils: a) Villa Beatriz, b) San Carlos, both farms located at the Líbano municipality, and c) La Estrella, Villahermosa municipality, Tolima Department (Colombia). In this figure, letters in colors correspond to: Q, quartz; H, hematite; G, goethite; I ilmenite; F Na Na-feldspar; M muscovite; O orthoclase; MI microcline; C calcite; and F ferrihydrite.

Table 4 relates reflection angles and intensities for the minerals present in the sample. Moreover, the interplanar distance (I.D.) is shown along with the Miller indices (Pierret, 1989) of each crystallographic plane.

The diffractogram of sample D2 (Figure 4b, Table 5) is like D1, hematite is present but with lower intensities (0.3072, 0.2225, 0.225). Goethite is present in greater quantities than D1, with a similar first peak and intensity. (D1 I = 0.4667; P = 2.8953 Å, D2 I = 0.4161; P = 21.8592 Å). The other goethite peaks present are well defined within the diffractogram with relevant intensities (0.3751, 0.1862, 0.2867, 01514) denoting a marked presence of this mineral. Like D1, ferrihydrite, is found in small quantities. An overlap of quartz and illite can also be observed in this sample, both with an interplanar distance of 3.37 Å, however a higher quartz intensity (0.7601) and a lower intensity for the illite (0.2867) is discernable. Sanidine or anorthoclase with relevant intensities (0.5221, 0.3051) was found, with an interplanar distance of 3.25 Å and 2.77 Å, respectively, as were albite-oligoclase, muscovite, illite and calcite.

Table 5. Crystallographic information of the peaks of mineral phases found in sample D2

Mineral name	Position	Intensity	Miller Index (H K L)	I.D (A)
Quartz (Q)	20.7783	0.2627	1 0 0	4.27
Goethite (G)	21.8592	0.4161	1 0 1	4.06
Na-feldspar (FNa)	22.7396	0.5628	1 0 0	3.84
Muscovite (M)	23.5825	0.4691	0 2 3	3.77
Hematite (H)	24.3604	0.3072	0 1 2	3.65
Muscovite (M)	25.4292	0.3098	-1 1 4	3.5
Quartz (Q)	26.4362	0.7601	0 1 1	3.37
Illite (I)	26.4213	0.2867	0 2 2	3.37
Orthoclase (O)	27.66	0.5221	0 4 2	3.25
Muscovite (M)	28.3467	0.4533	-1 1 5	3.14
Calcite (C)	29.4877	0.3388	1 0 4	3.03
Orthoclase (O)	32.6397	0.3051	-1 3 2	2.77
Illite (I)	35.6447	0.2955	2 0 0	2.51
Quartz (Q)	42.864	0.2351	2 0 0	2.12
Ferrihydrite (F)	45.1995	0.1538	1 0 3	1.97
Hematite (H)	49.7349	0.2225	0 2 4	1.83
Goethite (G)	50.7539	0.3751	1 1 2	1.79
Goethite (G)	53.2739	0.1862	2 1 2	1.71
Hematite (H)	54.5495	0.225	1 1 6	1.68
Quartz (Q)	55.5161	0.1849	0 1 3	1.65
Quartz (Q)	59.8721	0.2047	1 2 1	1.54
Ferrihydrite (F)	61.5306	0.1492	1 0 5	1.51
Ferrihydrite (F)	62.4578	0.1543	1 1 0	1.47
Goethite (G)	63.6514	0.2867	2 0 3	1.46
Illite (I)	67.7404	0.187	-2 4 5	1.38
Quartz (Q)	68.2719	0.1778	0 2 3	1.36
Goethite (G)	69.5441	0.1514	7 0 1	1.35

Sample D3 (Figure 4c, Table 6) shows a lower presence of oxide minerals, hematite is only reflected in a peak with an interplanar distance of 2.7 Å and an intensity of 0.2182. The concentration of goethite is low with interplanar distances of 4.15 Å, 2.17 Å at positions 21.019°, 41.7619°, respectively. As observed in the other samples, an overlap between quartz and illite is observed in this diffractogram, albeit with a lower intensity compared to the samples D1 and D2. Three additional overlaps are present: sanidine and orthoclase, both minerals with an interplanar distance of 3.19 Å, in which sanidine has an intensity of 0.2891 and orthoclase 0.2311; the second an overlap between sanidine, orthoclase and microcline all with an interplanar distance of 2.33 Å and intensities of 0.5323, 0.4628, 0.2337, respectively; and a third overlap between calcite and muscovite with intensities of 0.1484 for calcite and 0.1065

for muscovite, both with an interplanar distance of 1.87 Å. Muscovite and quartz are abundantly present in the sample, reflected in very well-defined peaks with relatively high intensities. The Table 7 provide Information on the crystalline structure and network parameters of main discriminated minerals.

Table 6. Crystallographic information of the peaks of mineral phases found in sample D3

Mineral name	Position	Intensity	Miller Index (H K L)	I.D (A)
Ferrihydrite (F)	18.1451	0.183	0 0 2	4.88
Quartz (Q)	20.9441	0.1988	1 0 0	4.24
Goethite (G)	21.0190	0.3175	1 0 1	4.15
Na-feldspar (F Na)	22.0274	0.3175	1 0 0	3.84
Muscovite (M)	23.7513	0.2327	0 2 3	3.74
Orthoclase (O)	25.6915	0.2985	-1 1 2	3.46
Quartz (Q)	26.5976	0.2406	1 0 1	3.35
Illite (I)	26.5332	0.1795	0 2 2	3.35
Sanidine (S)	27.8811	0.2891	-2 0 2	3.19
Orthoclase (O)	27.8814	0.2311	-2 0 2	3.19
Muscovite (M)	28.5265	0.2449	-1 1 5	3.12
Illite (I)	30.4259	0.2474	-1 1 3	2.93
Hematite (H)	33.0678	0.2182	1 0 4	2.7
Illite (I)	34.6052	0.1926	-2 0 1	2.59
Ferrihydrite (F)	35.5485	0.1727	1 0 0	2.52
Sanidine (S)	38.5325	0.5323	-1 1 3	2.33
Orthoclase (O)	38.5242	0.4628	-1 1 3	2.33
Microcline (MI)	38.5726	0.2337	-1 1 3	2.33
Quartz (Q)	39.7190	0.1516	1 1 1	2.26
Quartz (Q)	40.5794	0.1447	1 1 1	2.22
Goethite (G)	41.7619	0.1635	4 0 1	2.17
Muscovite (M)	44.3541	0.1586	-2 2 5	2.04
Quartz (Q)	45.5363	0.2251	0 2 1	1.99
Calcite (Ca)	48.4306	0.1484	1 1 6	1.87
Muscovite (M)	48.4387	0.1065	1 3 7	1.87
Quartz (Q)	50.1852	0.1366	1 1 2	1.81
Muscovite (M)	52.4450	0.1633	-2 2 8	1.74
Quartz (Q)	59.4935	0.1033	2 1 1	1.55
Muscovite (M)	60.7562	0.2733	-1 3 11	1.52
Ferrihydrite (F)	62.3980	0.1116	1 1 0	1.48

Table 7. Information on the crystalline structure and network parameters of each mineral

Mineral	Crystalline structure	a (Å)	b (Å)	c (Å)
Quartz (Q)	Trigonal	4.9160	4.9160	5.4054
Goethite (G)	orthorhombic	9.9134	3.0128	4.5800
Na-feldspar (F Na)	Trigonal	3.7670	3.7670	6.1540
Hematite (H)	Trigonal	5.0380	5.0380	13.7720
Muscovite (M)	Monoclinic	5.1988	9.0266	20.1058
Illite (I)	Monoclinic	5.2021	8.9797	10.2260
Sanidine (S)	Monoclinic	8.5160	13.0230	7.2060
Monoclinic (Mo)	Monoclinic	8.5440	13.0300	7.1950
Microcline (MI)	Triclinic	8.5784	12.9600	7.2112
Calcite (Ca)	Rhombohedral	4.9900	4.9900	17.0615
Ferrihydrite (F)	Trigonal	2.9550	2.9550	9.3700

4.3 Mössbauer Spectrometry

Magnetic analysis of the homogenized soil samples by Mössbauer spectroscopy, allowed a detailed and selective analysis of their mineralogical composition. This type of analysis is central to the identification of the octahedral structural sites that are occupied by the different cations of Fe, considering its hyperfine parameters. Results for the samples suggest two paramagnetic doublets with mineral phases containing Fe^{+2} and Fe^{+3}. The Fe^{+2} can be assigned to magnetite and ilmenite and 2:1 clay. In contrast, Fe^{+3} can be associated with hematite, goethite and ferrihydrite that were identified by the X-ray diffraction technique.

Table 8 summarizes the hyperfine parameters obtained for the three samples. In this table, the isomeric shift is indicated by IS, the line width by LW, the intensity by H1, the quadrupole splitting by SQ and A is the area. The MOSFIT (The Modular Open Source Fitter for Transients), a Python 2.7/3.x package for fitting, sharing, and estimating the parameters of transients, was used. For sample D1, two paramagnetic doublets are identified, which indicate the presence of magnetic crystalline Fe sites belonging to Fe^{+2} and Fe^{+3} and can be attributed to the presence of oxide minerals. For this sample, the clay minerals in the valence state of Fe^{+2} is found in a greater quantity covering an area of 56.11%, with an isomeric shift of 0.409 mms^{-1}, leaving hematite in the background, which presents a valence state of Fe^{+3} and covers an area of 43.89% with an isomeric shift of 1.094 mms^{-1}.

For sample D2, two paramagnetic doublets are also discriminated, similar to those presented in the previous sample, ferrous clay minerals, magnetite, ilmenite (Fe^{+2}) and goethite, hematite (Fe^{+3}) are also present.

The sample D3 show a single paramagnetic doublet corresponding to goethite but unlike the previous samples, them the valence state of this oxide mineral is Fe^{+3}, which has an isomeric deviation of 0.227 mms^{-1} and covers an area of 100% of the sample.

Samples D1 and D2 (Figure 5) exhibit similar spectra but different intensities per area, where two paramagnetic doublets were discriminated, and associated with the presence of goethite and hematite (Fe^{+3}). Such minerals are recognized as beneficial to the absorption of nutrients by plants. Similarities in these spectra are due to the geographic proximity of the farms, thus soil mineral content has been altered, facilitating the accumulation of similar oxide minerals.

The presence of Fe^{+3} in these three samples suggests that this state of valence of iron is precipitated as oxide and hydroxide. Then, this released iron is incorporated into lamellar silicates such as clays. Subsequent mixing with soil organic matter leads to reduction of ferric iron to ferrous iron (e.g. magnetite, ilmenite or wüstite). The presence of Fe^{+2} is attributed to magnetite and ilmenite the common soil oxides in this study's agro-ecological conditions, however ferrous clay minerals are also present. Fe^{+3} corresponds to goethite and hematite which are directly associated with soils in tropical areas where temperatures and pH facilitate its formation.

4.4 Remote sensing

High content of magnetite, ilmenite and hydroxyl bearing alteration are associated with laharic mud deposits from the last eruptions of the Nevado del
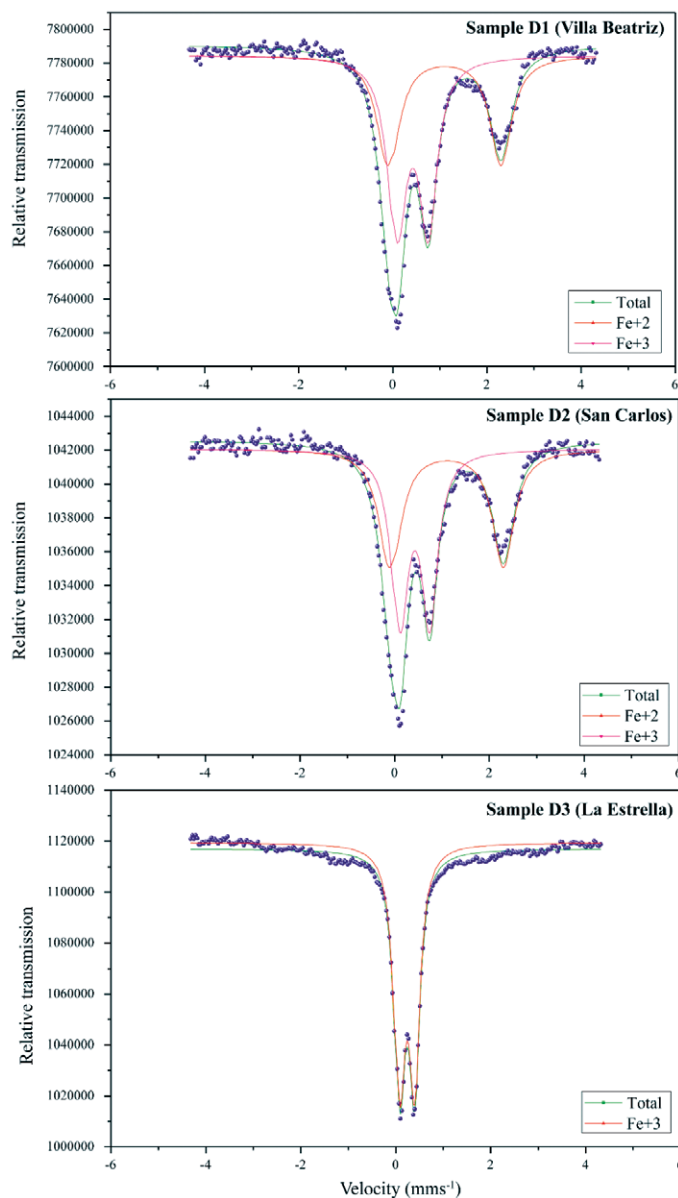
Figure 5. Mössbauer spectra of coffee crop soil A horizons: a) D1: Villa Beatriz farm, b) D2: San Carlos, both farms located at the Líbano municipality and c) D3: La Estrella at the Villahermosa municipality.

Table 8. Hyperfine parameters obtained for the different samples

Sample	Doublet	IS (mms^{-1})	LW (mms^{-1})	H1 (coups)	SQ (mms^{-1})	Area (%)
D1 (Villa Beatriz)	Magnetite 1 (Fe+2)	0.403 ± 0.0391	0.230 ± 0.0514	200729219 ± 0.0333	0.650 ± 0.0671	56.11
	Hematite 2 (Fe+3)	1.088 ± 0.0627	0.280 ± 0.0103	129102219 ± 0.0300	2.370 ± 0.0000	43.89
D2 (San Carlos)	Magnetite 1 (Fe+2)	0.403 ± 0.0380	0.205 ± 0.0490	19882527 ± 0.0364	0.622 ± 0.0663	51.47
	Hematite 1 (Fe+3)	1.084 ± 0.0589	0.277 ± 0.0987	13874722 ± 0.0314	2.370 ± 0.0000	48.53
D3 (La Estrella)	Goethite 1 (Fe+3)	0.221 ± 0.0160	0.135 ± 0.0218	178930859 ± 0.0217	0.309 ± 0.0217	100

Ruiz volcano on November 13, 1985. This can be observed around the volcanic cone, where a high abundance of these minerals was detected using specific bands present in the Sentinel-2A Satellite Sensor MSI which covers 13 spectral bands (443–2190 nm) (Figure 6). So, Fe^{+2} is in the form of magnetite or ilmenite that has not had enough time to decompose, because they are relatively stable; also, in pyroclastic and lahars so young, it is possible that Fe^{+2} is in its mineral form as biotite or hornblende.

Large parts of these volcanic rock units fall into the image pixels that are covered by vegetation, and thus masked out for analysis (Figure 6A, 7A, 7C). The San Carlos and Villa Beatriz farms are dominated by a thick vegetation cover that masks the spectral response of the minerals present (Figure 6B). Despite the closeness of the farms and the small area, the synoptic analysis provided by the Sentinel data, our analyses suggest that different spectral signatures related to oxide and hydroxyl bearing iron phases could be discriminated (Figure 7-B). In contrast, in the La Estrella farm, the abundance of iron oxide-related minerals is much lower (Figure 7-D). Although the images show areas of exposed soil which are not affected by the vegetation cover, the detection of iron mineralization is almost negligible. In urban areas, our Sentinel analyses show false positives, which constitute an anomaly since a large amount of infrastructure (buildings, vehicles, water pipes, etc) is concentrated in these areas. Recent studies have demonstrated the Sentinel's high sensitivity to Iron include depth discrimination of mines located near urban areas (Mielke et al., 2014). The present investigation confirms the high sensitivity of these analyses to detect such structures.

5. Discussion

The soils of the three farms selected for this study are inceptisols (Figure 1) derived principally from volcanic deposits and sedimentary lithic fragments. Thus, the parent material is expected to be similar. Our study shows significant differences across analyzed sites may linked to the proximity of the farm to the volcano. Unfortunately, the number of farms considered in this work was not significant enough to relate farm agricultural practices with coffee soil production. Detecting these compositional differences in the same soil type is not a simple task, and the multi-method approach used in this research allowed the detection of such differences.

Results indicate the presence of Fe^{+2} and Fe^{+3} mineral phases based on ambient temperature spectra and paramagnetic doublets for all samples. The X-ray diffraction identified iron oxide mineral phases, as well as the recognition of other minerals such as feldspars, quartz, phyllosilicates, and carbonates. For the Villa Beatriz (D1), a varied mineralogy (calcite, illite, quartz and muscovite) was identified, although oxide minerals such as hematite and goethite appear in small proportions. The San Carlos farm (D2) has a soil rich in minerals, in addition to calcite, illite, quartz and muscovite that were present in sample D1, other minerals in D2 such as: orthoclase, hematite, goethite and ferrihydrite are present in notable quantities, suggesting a fertile soil. The soils of the La Estrella farm (D3) are the most mineralogically diverse containing: feldspars such as sanidine, microcline and orthoclase, which indicate that the fertility of this soil is very high, because and together with the organic load, they favor the correct development of plants.

Diverse studies have shown that Fe and Al oxide minerals are important regulators for the stabilization of a soil's organic content (SOC) in oxisols (Kleber et al., 2005; Zhang et al., 2010; Ye et al., 2017). In the soils analyzed here, Fe and Na oxide minerals were found but not Al; additionally, soils in our study area have a very low organic matter content (SOM), which is typical of inceptisols in tropical and humid areas (Igwe et al., 2010). From our remote sensing analysis with Sentinel-2A data, we observed a regional signal from bandwiths that indicate Hydroxyl bearing Iron and Ferrous oxides, which could explain the high acidity of soils, and this is consistent with our pH measurements (5.0 ± 0.5). In ice sheets or glaciers, the exchange between Hydroxyl-bearing minerals and water indicate effects of glacial erosion. During this process abrasion of clays and micas increases the number of broken bonds in the crystalline structure of the mineral, which promotes the development of cleavages and accelerates the rate at which these minerals exchange oxygen and hydrogen isotopes with water (Souchez et al., 1990). This explains the large-scale presence of hydroxyl-bearing minerals.

(B)
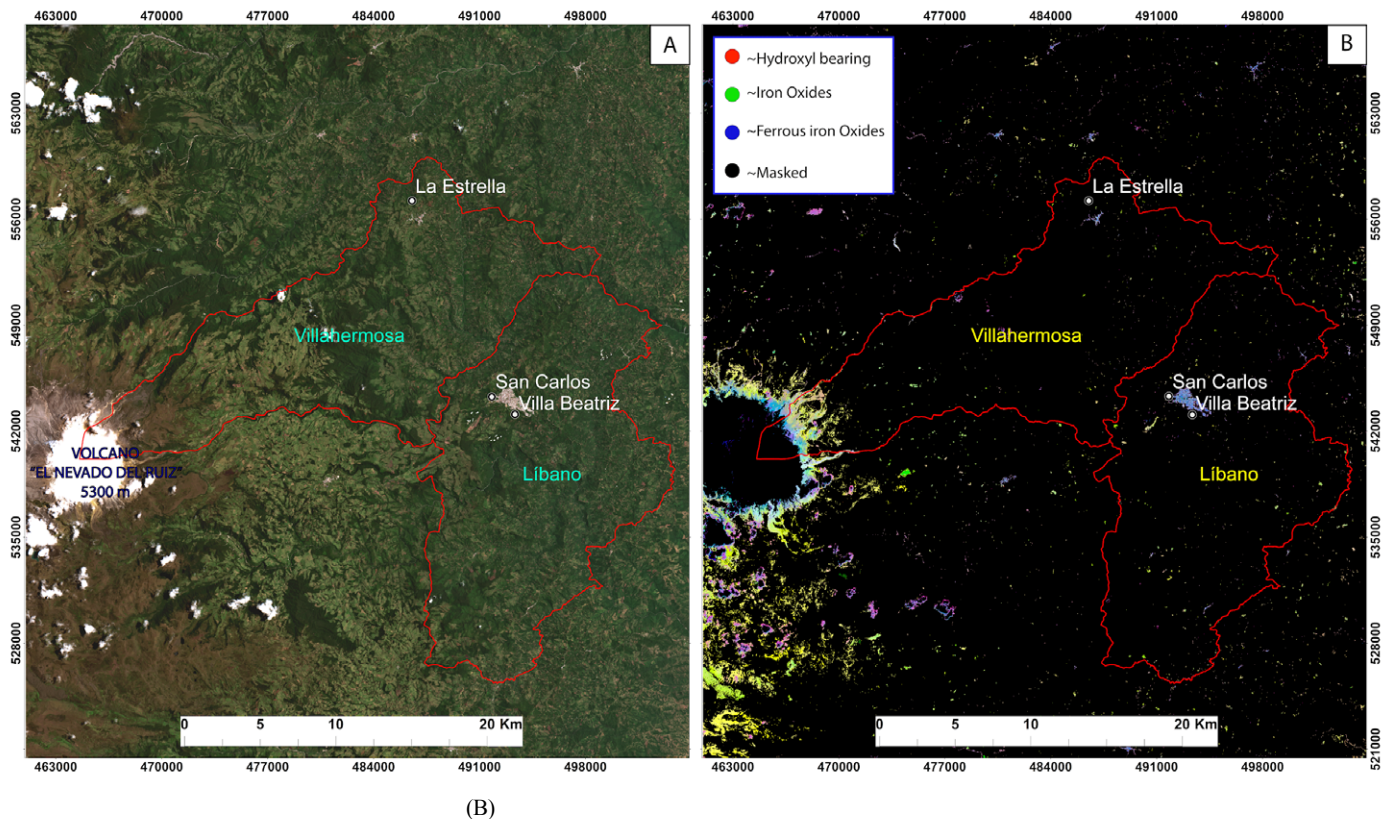
Figure 6. (A) Google image showing the position of the Nevado del Ruíz volcano with respect to the Villahermosa and Líbano towns. (B) A color composite (RGB: R: 4, G: 3, B:2) made with Sentinel-2A MSI, combination of band ratios 11/12 in red, 4/2 in green, and 4/11 in blue are showed.

Coffee plantation soil characterization using a multi-method approach near the Volcano Nevado del Ruiz, Colombian Central Cordillera

271
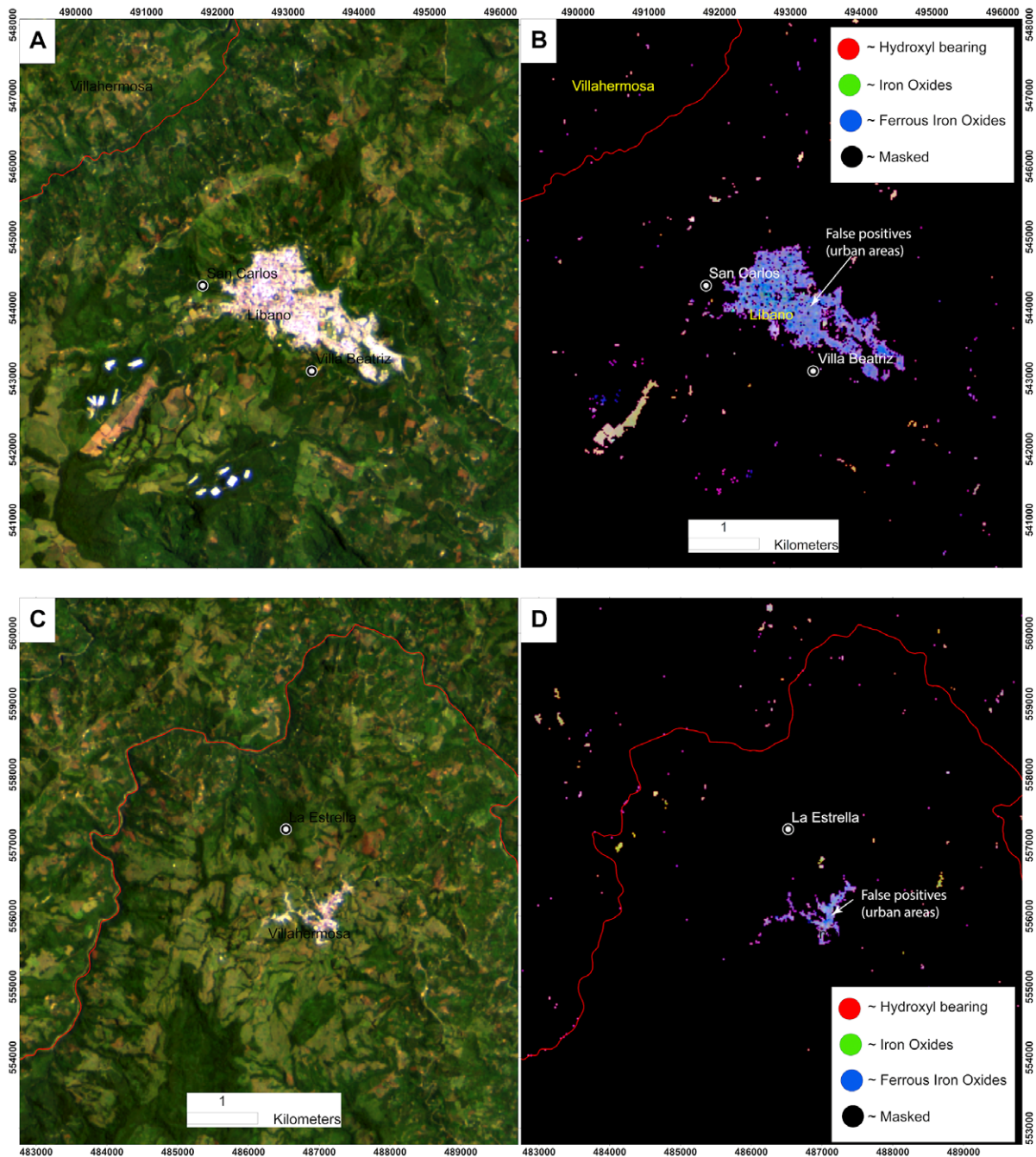
Figure 7. A color composite (RGB: R: 4, G: 3, B:2) made with Sentinel-2A MSI (A-C) for the San Carlos, Villa Beatriz and La Estrella farms. Combination of bandwidths 11/12 in Red, 4/2 in Green and 4/11 in blue (B-D).

Our results demonstrate the existence of a large ice cover that could have accelerated the rate of exchange between hydroxyl-bearing minerals and water. Additionally, our remote sensing analysis is sensitive enough to detect anomalies of iron oxides in large flat surfaces corresponding to cities, but also, those flat surfaces could correspond with topographic remnants that have been preserved by the different volcanic episodes.

6. Conclusions

Mössbauer spectroscopy selectively identifies iron-bearing mineral phases in coffee-growing soils by determining the presence of Fe^{+2} and Fe^{+3}, where the latter was more prevalent. The application of this technique allowed identification of mineral phases such as magnetite, ilmenite, hematite and goethite which were also independently identified by X-ray diffraction. The presence of Fe^{+2} in the form of magnetite or ilmenite suggests that soils have not had time to decompose, because they are relatively stable; also, in pyroclastic and lahars so young it is possible that Fe^{+2} is derived from rock forming minerals biotite and hornblende.

In addition to the abundant presence of quartz, feldspars such as sanidine, microcline, orthoclase and sodium feldspars were found, which belong to the group of tectosilicate minerals, as well as phyllosilicate minerals such as illite and biotite.

The different agricultural practices applied in the sampled productive region could have had an influence on the quality of the soils, since it is evident that those that deploy environmentally friendly practices had a greater quantity

of feldspars which are linked to the abundance of organic matter and this in turn is related to good soil quality. However, the fertility of minerals for the soil around farms is due to the proximity to the volcano, rather than to the organic matter content. The differences observed between these three farms have also been observed in other municipalities in the department of Tolima, such as in Ibagué and Santa Isabel (Bustos-Rodríguez et al., 2012) where the northernmost farms exhibit minor presence of Fe^{+2}.

The physical-chemical analyses of the soils sampled for iron (Fe) vary from low (4 to 5 mg/kg) to adequate/high (23 to 25 mg/kg). The pH data were found to be within acceptable levels for coffee cultivation. This work demonstrates the usefulness band-specific ratios of Sentinel-2 MSI data for the detection of areas with high surface iron content. Remote sensing methodology can be applied cost-effectively in larger regions of Colombia and can provide interesting insights into the possibility of detecting new areas for the cultivation of high-quality coffee.

To increase the reliability of the study, it is recommended to increase the number of samples and production systems to be sure that the agricultural practices carried out contribute to the quality and sustainability of the soils. It is suggested that the measurements be made by Mössbauer spectroscopy at different temperatures to be able to appreciate other oxide minerals that are not evident at room temperature. In addition, it is necessary to carry out a detailed study of inceptisols from similar parent material, in non-cultivated regions. This allow to have a frame of reference on the process of soil degradation and the influence of different agricultural practices.

Acknowledgements

References

Bermúdez-Valderrama, L. P., & Gaitán-Díaz, N. A. (2016). *Evaluación de nematodos de vida libre como indicadores de calidad y salud de suelos cafeteros*. Trabajo de Grado en Administración Ambiental, Universidad de Ibagué, 110 p.

Bustos-Rodríguez, H., Oyola-Lozano, D., Rojas-Martínez, Y. A., Rivera-Pinilla. M., & Pérez-Alcázar, G. A. (2012). Characterization of mineral phases of agricultural soil samples of Colombian coffee using Mössbauer spectroscopy and X-ray diffraction. *Hyperfine Interact*, 208, 13–18, DOI 10.1007/s10751-012-0573-z.

Byrne, J., & Kappler, A. (2019). Mössbauer Spectroscopy. In: J. Kenney, H. Veeramani, & D. Alessi (Eds.) *Analytical Geomicrobiology: A Handbook of Instrumental Techniques* (pp. 314-338). Cambridge: Cambridge University Press. DOI:10.1017/9781107707399.013

Ciampalini, A., Garfagnoli, F., Antonielli, B., Moretti, S., & Righini, G. (2013). Remote sensing techniques using Landsat ETM+ applied to the detection of iron ore deposits in Western Africa. *Arabian Journal of Geosciences*, 6, 4529-4546, DOI:10.1007/s12517-012-0725-0.

Colombo, C., Palumbo, G., He, J. Z., Pinton, R., & Cesco, S. (2013). Review on iron availability in soil: interaction of Fe minerals, plants, and microbes. *Journal of Soils and Sediments*, 14, 538. https://doi.org/10.1007/s11368-013-0814-z

CCDIA-Corporación Colombiana De Investigación Agropecuaria. (2005). *Guía para la toma de muestras de suelos ICA*. Bogotá: Primera edición, p. 56-59.

Clark, M. S., Horwath, W. R., Shennan, C., & Scow, K. M. (1998). Changes in Soil Chemical Properties Resulting from Organic and Low-Input Farming Practices. *Agronomy Journal*, 90, 662–671. DOI:10.2134/agronj1998.00021962009000050016x

Clark, R. B., & Baligar, V. C. (2000). Acidic and alkaline soil constraints on plant mineral nutrition. In: R. E. Wilkinson (Ed.). *Plant-environment interaction*. New York: Marcel Dekker. pp. 133–177.

Cudahy, T., & Hewson, R. (2002). *ASTER Geological Case Histories: Porphyry-Skarn-Epithermal, Iron Oxide Cu–Au and Broken Hill Pb–Zn–Ag*. Communication in the Workshop Mapping the Earth with ASTER, London.

Downs, R. T., & Hall-Wallace, M. (2003). The American Mineralogist crystal structure database. *American Mineralogist*, 88(1), 247–250.

Eswaran, H., & Reich, P. (2005). Global Soil Regions. 1: 130,000,000. Global Soil Suborder Map 1, 5,000,000 http://soils.usda.gov/use/worldsoils/mapindex/order.html.

Fink, J. R., Vasconcellos Inda, A., Tales, T., & Vidal, B. (2016). Iron oxides and organic matter on soil phosphorus availability. *Ciência e Agrotecnologia*, 40(4), 369-379. https://doi.org/10.1590/1413-70542016404023016

Guarin, L. A. (2004). *Variación pedogenética en los materiales de sedimentos de Lahar que sepultaron Armero, Tolima en 1985*. Bogotá: Tesis de Postgrado, Universidad Nacional, 103 p.

Hernández, J., & Meurer, E. (1997). Óxidos de hierro en los suelos: sus propiedades y su caracterización con énfasis en los estudios de retención de fósforo. *Agrociencia*, 1(1), 1–14.

Igwe, C. A., Zarei, M., & Stahr, K. (2010). Fe and Al oxides distribution in some ultisols and inceptisols of southeastern Nigeria in relation to soil total phosphorus. *Environmental Earth Sciences*, 60(5), 1103-1111. https://doi.org/10.1007/s12665-009-0254-7

Kang, Y., Khan, S., & Ma, X. (2009). Climate change impacts on crop yield, crop water productivity and food security – A review. *Progress in Natural Science*, 19(12), 1665–1674. https://doi.org/10.1016/j.pnsc.2009.08.001.

Larson, A. C., & Von Dreele, R. B. (2004). General Structure Analysis System (GSAS). Los Alamos National Laboratory, Report LAUR 86–748.

Li, W., & Lan, P. (2017). The Understanding of the Plant Iron Deficiency Responses in Strategy I Plants and the Role of Ethylene in This Process by Omic Approaches. *Frontiers in plant science*, 8, 40. DOI:10.3389/fpls.2017.00040

Lindsay, W. (1991). Iron oxide solubilization by organic matter and its effect on iron availability. Plant and Soil, 130(1/2), 27-34. Retrieved from http://www.jstor.org/stable/42937282

Louis, J., Debaecker, V., Pflug, B., Main-Knorn, M., Bieniarz, J., Mueller-Wilm, U., Cadau, E., & Gascon, F. (2016). Sentinel-2 Sen2Cor: L2A Processor for Users, Proceedings Living Planet Symposium 2016. Spacebooks Online, pp. 1–8.

Mielke, C., Boesche, N. K., Rogass, C., Kaufmann, H., Gauert, C., & De Wit, M. (2014). Spaceborne Mine Waste Mineralogy Monitoring in South Africa, Applications for Modern Push-Broom Missions: Hyperion/OLI and EnMAP/Sentinel-2. Remote Sensing, 6(8), 6790-6816. DOI:10.3390/rs6086790

Nenova, V. (2006). Effect of iron supply on growth and photosystem II efficiency of pea plants. *General and Applied Plant Physiology*. (Special Issue) 32, 81-90.

Pierret, R. F. (1989). *Semiconductor fundamentals volume I, modular series on solid state devices*. Second edition, 10–13.

Reddy, B. V. S., Sanjana-Reddy, P., Bidinger, F., & Blümmel, M. (2003). Crop management factors influencing yield and quality of crop residues. *Field Crops Research*, 84(1–2), 57–77. https://doi.org/10.1016/S0378-4290(03)00141-2.

Rout, G. R., & Sahoo, S. (2015). Role of iron in plant growth and metabolism. *Reviews in Agricultural Science*, 3, 1–24. DOI:10.7831/ras.3.1

Ruan, H. (2014). Analysis of Major Factors Influencing Crop Yield of Shandong

Coffee plantation soil characterization using a multi-method approach near the Volcano Nevado del Ruiz, Colombian Central Cordillera

273

Province. In: Xu S. (Ed.) Proceedings of Selected Articles of 2013 World Agricultural Outlook Conference. Springer, Berlin, Heidelberg.

Sabins, F. F. (1999). Remote sensing for mineral exploration. *Ore Geology Reviews*, 14(3-4), 157-183. https://doi.org/10.1016/S0169-1368(99)00007-4

Shenker, M., & Chen, Y. (2005). Increasing Iron Availability to Crops: Fertilizers, Organo-Fertilizers, and Biological Approaches. *Soil Science & Plant Nutrition*, 51, 1–17. DOI:10.1111/j.1747-0765.2005. tb00001.x

Sadeghian, S. (2008). Fertilidad del suelo y nutrición del café en Colombia. *Boletín técnico* N° 32 Cenicafé.

Souchez, R., Lemmens, M., Lorrain, R., Tisson, J.-L., & Sugden, D. (1990). Influence of hydroxyl-bearing minerals on the isotopic composition of ice from the basal zone of an ice sheet. *Nature*, 345(6272), 244-246. https://doi.org/10.1038/345244a0

Van der Meer, F. D., Van der Werff, H. M. A., & Van Ruitenbeek, F. J. A. (2014). Potential of ESA's Sentinel-2 for geological applications. *Remote Sensing of Environment,* 148, 124-133. https://doi.org/10.1016/j. rse.2014.03.022

Van der Werff, H., & Van der Meer, F. (2016). Sentinel-2A MSI and Landsat 8 OLI Provide Data Continuity for Geological Remote Sensing. Remote Sensing 8, 883. DOI:10.3390/rs8110883.

Varret, F., & Teillet, J. (1976). Unpublished MOSFIT program.

Zhang X., Wang, L., Wang, L., Liu, B., Zheng, J., Zhao, J., Santana, G.P., Fabris, J. D., Goulart, A. T., & Santana, D. P. (2001). Magnetite and its transformation to hematite in a soil derived from steatite. *Revista Brasileira de Ciencia do Solo*, 25, 33–42.